Journal of Ceramic Processing Research. Vol. 19, No. 5, pp. 413~418 (2018)

J O U R N A L O F
Ceramic Processing Research

Effects of binary conductive additives on electrochemical performance of a sheet-type composite cathode with different weight ratios of $LiNi_{0.6}Co_{0.2}Mn_{0.2}O_2$ in all-solid-state lithium batteries

Jiu Ann, Sunho Choi, Jiyae Do, Seungwoo Lim and Dongwook Shin*
Division of Materials Science and Engineering, Hanyang University, 222 Wangsimni-ro, Seongdong-gu, Seoul133-791, Korea

All-solid-state lithium batteries (ASSBs) using inorganic sulfide-based solid electrolytes are considered prospective alternatives to existing liquid electrolyte-based batteries owing to benefits such as non-flammability. However, it is difficult to form a favorable solid-solid interface among electrode constituents because all the constituents are solid particles. It is important to form an effective electron conduction network in composite cathode while increasing utilization of active materials and not blocking the lithium ion path, resulting in excellent cell performance. In this study, a mixture of fibrous VGCF and spherical nano-sized Super P was used to improve rate performance by fabricating valid conduction paths in composite cathodes. Then, composite cathodes of ASSBs containing 70% and 80% active materials ($LiNi_{0.6}Co_{0.2}Mn_{0.2}O_2$) were prepared by a solution-based process to achieve uniform dispersion of the electrode components in the slurry. We investigated the influence of binary carbon additives in the cathode of all-solid-state batteries to improve rate performance by constructing an effective electron conduction network.

Key words: Conductive additive mixture, Solution-based process, Sulfide solid electrolyte, All-solid-state battery.

Introduction

Recently, demand for batteries of high capacity and long cycle life has been driven by electric vehicles (EVs) and energy storage systems (ESSs) as part of the effort to adopt renewable energy sources over fossil fuels. Typical lithium ion batteries (LIBs) based on organic liquid electrolyte carry the risk of explosion. All-solid-state batteries (ASSBs) can resolve the safety issue by using non-flammable solid electrolyte, which also carries the benefit of superior mechanical properties [1, 2]. Owing to development of sulfide-based solid electrolyte, it is feasible to increase the lithium ion conductivity of ASSBs to that of liquid-based batteries, improving ASSB energy density. Moreover, as all-solid-state batteries exhibit temperature stability in extreme conditions, ASSBs are expected to be applied in diverse fields [3-5].

Since composite electrodes of all-solid-state batteries are composed by dry-mixing active material, solid electrolyte, and conductive additive, it is difficult to achieve a well distributed contact network among the three components due to their solid states [6]. Forming good lithium ion paths and electron paths at the particle-particle interface is complicated and can have adverse implications on cell performance in cycle life and rate capability. Thus, modification to optimize the solid-solid interface in composite electrodes is indispensable to operation of high performance all-solid-state batteries.

One simple way to improve cycle performance and rate capability is to enhance electron conductivity of the electrode [7]. Although cathode active materials such as $LiFePO_4$ (LFP) and $LiNi_xCo_yMn_zO_2$ (NCM, x+y+z=1) suffer from poor innate electron conductivity, the use of conductive additives possessing good electron conductivity in these and other composite cathode materials alleviates their intrinsic limit in cell performance [8]. An effective conductive network among active materials can be constructed by carbon sources, which can occupy a small proportion of the composite due to their large surface area and outstanding conductivity. Thus, solid electrolyte with an ion conducting path is sufficiently contained in a composite cathode in all-solid-state batteries. However, either too large or too small a proportion of conductive additive leads to restricted utilization of active material. At the extreme of no conductive additive, the electrochemical reaction deactivates [9]. Super P, which is spherical nano-sized carbon material, has generally been used as conductive additive, but its self-agglomeration is a big disadvantage [10]. Alternatively, extending contact area with active materials, fibers, or flake type carbon materials such as VGCFs (vapor grown carbon fibers), CNTs (carbon nanotubes), and graphite has been investigated as conductive additives to enhance cell

*Corresponding author:
Tel : +82-2-2220-0503
Fax: +82-2-2220-4011
E-mail: dwshin@hanyang.ac.kr

performance [11-13].

To date, it has been necessary to fabricate scalable sheet-type electrode in all-solid-state-batteries for practical applications like EVs [14-17]. However, addition of non-conductive polymeric binder in slurry-based electrode can result in poor rate performance by blocking ion and electron conduction paths [18]. In this study, for the first time, the effect of binary conductive additive on the rate performance of all-solid-state batteries fabricated by a sheet-type composite cathode with different contents of NCM active materials was studied.

Experimental

Synthesis of Li_6PS_5Cl solid electrolyte powder - The Li_6PS_5Cl solid electrolyte was prepared by high energy mechanical milling using Li_2S (Alfa Aesar), P_2S_5 (Sigma Aldrich), and LiCl (Sigma Aldrich) in stoichiometric molar ratio [19]. The starting materials were ball milled at 600 rpm for 40 hrs using a high energy planetary ball mill (Pulverisette 7, Fritsch). As-synthetized Li_6PS_5Cl powder was heated at 550 °C for 5 hrs under an argon atmosphere.

Fabrication of ASSB half cells using a cathode sheet prepared by slurry mixture-The cathode sheet was fabricated by mixing composite material consisting of active materials, solid-electrolytes, conductive additives, and polymeric binder in o-xylene solvent. The constituents of the composite were, respectively, $LiNbO_3$-coated $LiNi_{0.6}Co_{0.2}Mn_{0.2}O_2$ (NCM 622), Li_6PS_5Cl, VGCF (Showa Denko)/ Super P (Timcal), and nitrile-butadiene rubber (NBR, abt. 10wt% o-xylene). The composite cathodes (NCM622:Li_6PS_5 Cl:Super-P/VGCF:NBR) were evaluated at weight percentages of 68.1/9.2/1.3/1.4 and 77.8/19.5/1.4/1.3. The total content of conductive additives was fixed at 1.3 wt%, and the mixture of VGCF:Super P was portioned out at 0:3, 1:2, 2:1, 3:0, which will be referred to as SS, SV, VS, and VV in the text, respectively. The slurry was coated on aluminum foil using a doctor blade and then dried at 120 °C for 2 hrs under vacuum [20]. To assemble the all-solid-state half-cell, solid electrolyte powder was pressed at 20 MPa in a PTEF (polytetrafluoroethylene) mold of 13 mm diameter. The prepared cathode sheet and Li-In powder as counter electrode were attached on either side of the solid electrolyte layers, followed by pelletizing at 45 MPa. All processes were performed in an Ar-filled glove box ([H_2O] < 1 ppm).

Material and electrochemical characterization-The morphology of the composite cathode surface containing 70% and 80% NCM 622 with different carbon additives was observed using a field emission scanning electron microscope (Fe-SEM; S-4800, Hitachi). The electrochemical performance of the cells was evaluated at various current densities (0.1C-2C) at a cut off voltage of 2.38 V-3.68 V (vs. Li-In) at room temperature using a charge-discharge measurement device (TOSCAT-3100, Toyo System). Linear sweep voltammetry (LSV) and electrochemical impedance spectroscopy (EIS) measurements were performed.

Results and Discussion

The SEM images of the 70% NCM electrode sheet containing Super P and VGCF as a single conductive additive are shown in Fig. 1. As shown in the images, the NCM active material consisting of micro-sized secondary particles appears like a bunch of grapes organized by nano-sized primary particles. From Fig. 1(a), spherical nano-sized Super P can attach to an individual NCM particle due to its large surface area. But, Super P more readily self-aggregates, which impedes electrode conductivity by reducing the number of activated NCMs. On the other hand, fibrous VGCFs connect adjacent NCM particles as shown in Fig. 1(d), creating an electron bridge. VGCF, with its high aspect

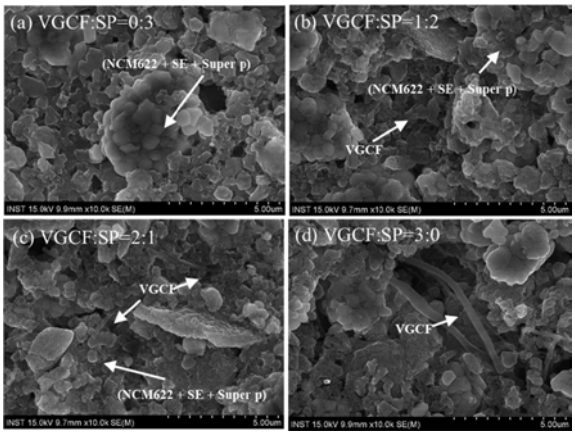

Fig. 1. SEM image of 70% NCM cathode using (a) SS, (b) SV, (c) VS and (d) VV as conductive additives.

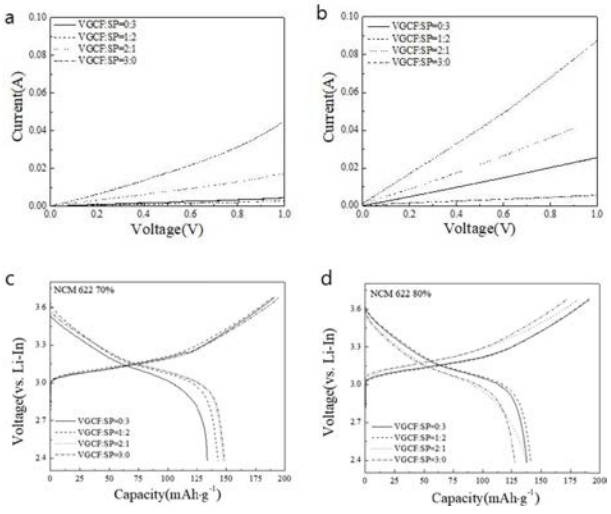

Fig. 2. Linear sweep voltammetry (LSV) curves of 70% and 80% NCM composite cathodes with different ratios of conductive additives (a, b) and initial charge/discharge curve of 70% and 80% (c, d).

ratio, can utilize isolated active material particles surrounded by insulators (solid electrolytes and binder), such that electron conducting pathways are constructed over solid electrolytes. The NCM cathodes employing VGCF/SP binary conductive additives (Figs. 1(b) and 1(c)) show coexisting Super P and VGCF, which together construct short and long conduction paths. Different types of electron conducting paths were formed by diverse carbon additives in NCM composite cathode.

Electrochemical performance of cathode electrodes containing different fractions of VGCF/SP is shown in Fig. 2. The linear sweep voltammetry curves (LSV) for 70% and 80% NCM composite cathodes are shown (Fig. 2(a) and 2(b)). The dc resistance of cathode composites with different ratios of VGCF/Super P is indicated by LSV. To clearly compare the resistance values of all samples, cathode sheets of similar thickness and diameter were used, and electron conductivity of composite cathodes was calculated.

Electronic conductivity of VGCF is higher than that of Super P due to its higher degree of crystalline graphite. However, the conductive additive effects of VGCF and Super P on the cathodes varied with active material content. The 70% NCM cathode using VGCF as the single conductive additive demonstrated the lowest resistance value of 22 Ω compared to electrodes with SV (364 Ω), VS (60 Ω), and VV (234 Ω). The electron conductivity increased in the order of VV (8.9×10^{-4} S/cm) > VS (3.3×10^{-4} S/cm) > SS (8.4×10^{-5} S/cm) > SV (5.4×10^{-5} S/cm). Contrary to expectations, in 80% NCM cathodes, the electrode resistance was 39 Ω, 12 Ω, 22 Ω, and 187 Ω for electrodes with SS, SV, VS, and VV conductive additives, respectively. The electron conductivity followed the order of SV (9.1×10^{-4} S/cm) > VS (5.2×10^{-4} S/cm) > SS (4.2×10^{-4} S/cm) > VV (6.4×10^{-5} S/cm).

Fig. 2 shows charge-discharge curves of all-solid-state batteries with composite cathode prepared at 70% and 80% active material content at current density of 0.1 C. The cathode containing VGCF as the only carbon source had the highest capacity of 148 mAh g^{-1}, while that prepared with Super P had the lowest capacity of 134 mAh g^{-1}. The respective discharge capacities of VS and SV were 147 mAh g^{-1} and 143 mAh g^{-1}. However, the 80% NCM cathode with VV as the single conductive additive showed inferior discharge capacity of 128 mAh g^{-1}, suggesting a lack of contact points between NCM particles and VGCF particles. The 80% NCM cathode with VS, SV, and SS cathodes showed respective discharge capacities of 137 mAh g^{-1}, 141 mAh g^{-1}, and 138 mAh g^{-1}. These results indicate that the electron conductivity of the composite cathode is strongly related to cell performance.

The use of different conductive additives contributed to different interfacial resistances in the 70% NCM composite cathode. Electrochemical impedance spectroscopy (EIS) was performed after initially charging to 3.68 V Li-In at a current density of 0.1C in Fig. 3. The AC impedance spectra indicate the resistance of solid electrolyte, positive electrode, and negative electrode in the frequency region from 100 kHz to 1 Hz. All cathodes had similar solid electrolyte resistance (R_{SE}) by controlling the solid electrolyte layer to confirm the contributions of VGCF/Super P. As shown in Fig. 3, the semicircle that stands for the resistance of charge transfer (R_{ct}) between cathode and solid electrolyte interfaces is strongly affected by VGCF/Super P content [20, 21]. The cathode interfacial resistance values with VV, VS, SV, and SS were, respectively, 13 Ω, 18 Ω, 20 Ω, and 25 Ω. The composite cathode with VGCF showed the smallest R_{ct}, suggesting that the 70% NCM cathode with VGCF can derive effective ion and electron conduction paths.

The rate performance measurement for composite cathodes with 70% active material was carried out under different current densities from 0.1C to 2C. As expected, the cathode with VGCF showed outstanding

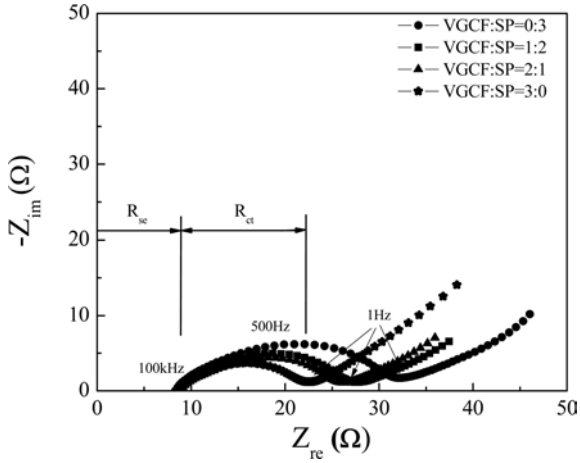

Fig. 3. Electrochemical impedance spectroscopy (EIS) of a 70% NCM cathode with different ratios of VGCF/SP.

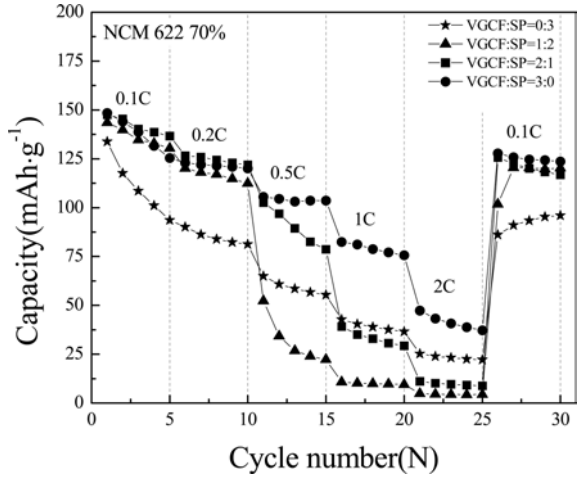

Fig. 4. Rate performance of a 70% NCM composite cathode using different ratios of binary conductive additives.

rate capability and cycle life under high current density, resulting from high electron conductivity and low charge transfer resistance (Fig. 2 and Fig. 3). The fibrous shape of VGCF fabricated a valid electron bridge between NCM particles. Meanwhile, the cathode with Super P showed inferior rate performance, suggesting that agglomeration of carbon sources hindered formation of ion and electron conduction paths. However, contrary to expectation, binary conductive additives of VGCF and Super P exhibited poor capacity fading at current densities higher than 0.5 C. This indicates that Super P is not acceptable in a 70% NCM cathode due to agglomeration. However, employing a sufficient amount of VGCF in the 70% NCM cathode led to construction of an effective conductive network between NCM particles despite its poor surface coverage property.

Cell performance with VGCF/SP as conductive additives in the 80% NCM cathode, however, was quite different from that of the 70% sample. With an increasing proportion of active material in the composite cathode, the interface of solid electrolyte and conductive additives is diminished, depleting the ion and electron conduction paths. Therefore, it is important to form a favorable interface between active material and conductive additives in cathodes of high active material content [22]. To confirm the relationship between cell resistance and rate capability, we measured the initial cycle impedance spectra of the 80% NCM cathode containing different ratios of VGCF/SP under low and high current densities (0.1C vs. 0.5C). As shown in Fig. 5 and Table 1, the cathode of binary conductive additives with more Super P (VGCF/SP 1:2) had the smallest R_{ct}, whereas that of VGCF only had the largest R_{ct}. At high current density (0.5 C), the charge transfer resistance (peak at 500 Hz) and the negative electrode resistance (peak at 1 Hz) increased, increasing total cell resistance and reducing electrochemical reaction [21, 23]. However, the SV revealed the lowest total resistance under 0.5 C rate, indicating that a certain content of binary carbon additive (VGCF/SP 1:2) can construct an effective electron conducting network in an 80% NCM cathode.

Compared to the 70% NCM cathode, the all-solid-state battery using SV binary conductive additive exhibited preferable rate performance to the 80% NCM cathode due to its superior electronic conductivity and the lowest charge transfer resistance. (Fig. 5(b) and Fig. 2(b)). Unfortunately, the electrodes with high VGCF content delivered poor rate capability. Moreover, at high current density of 0.5C, all samples showed inferior capacity retention because of increased total cell resistance (Fig. 5). A chronic problem of high content active material is encountered in electrodes of all-solid-state batteries because ion and electron conduction paths are hindered by lack of inactive materials to make good contact with active materials. Nevertheless, considering effects on the valid electron conductive network, the electrode-containing portion of VGCF/SP 1:2 exhibits

Table 1. Resistance values and discharge capacity of an 80% NCM cathode using different conductive additives at 0.1C and 0.5C after the first cycle.

Sample	$R_{se}(\Omega)$	$R_{ct}(\Omega)$		Discharge capacity ($mAhg^{-1}$)	
		0.1C	0.5C	0.1C	0.5C
VGCF:SP=0:3	12	30	34	138	82
VGCF:SP=1:2	12	20	26	141	79
VGCF:SP=2:1	12	32	35	137	21
VGCF:SP=3:0	12	45	50	128	41

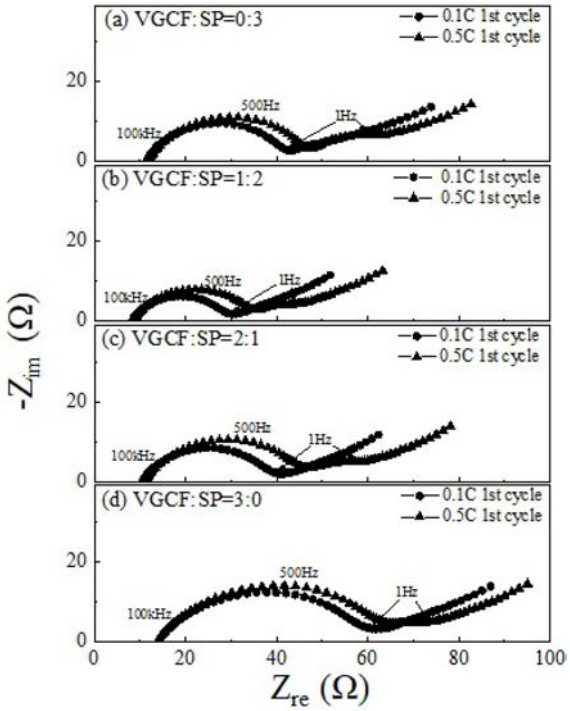

Fig. 5. EIS of the 80% NCM cathode at low and high current density (0.1C vs. 0.5C).

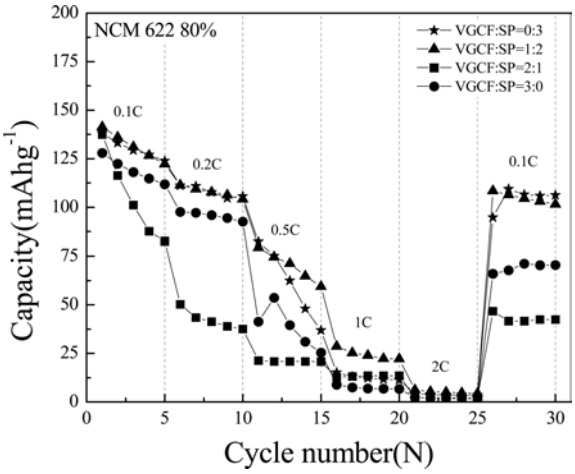

Fig. 6. Rate performance of the 80% NCM composite cathode using different ratios of binary conductive additives.

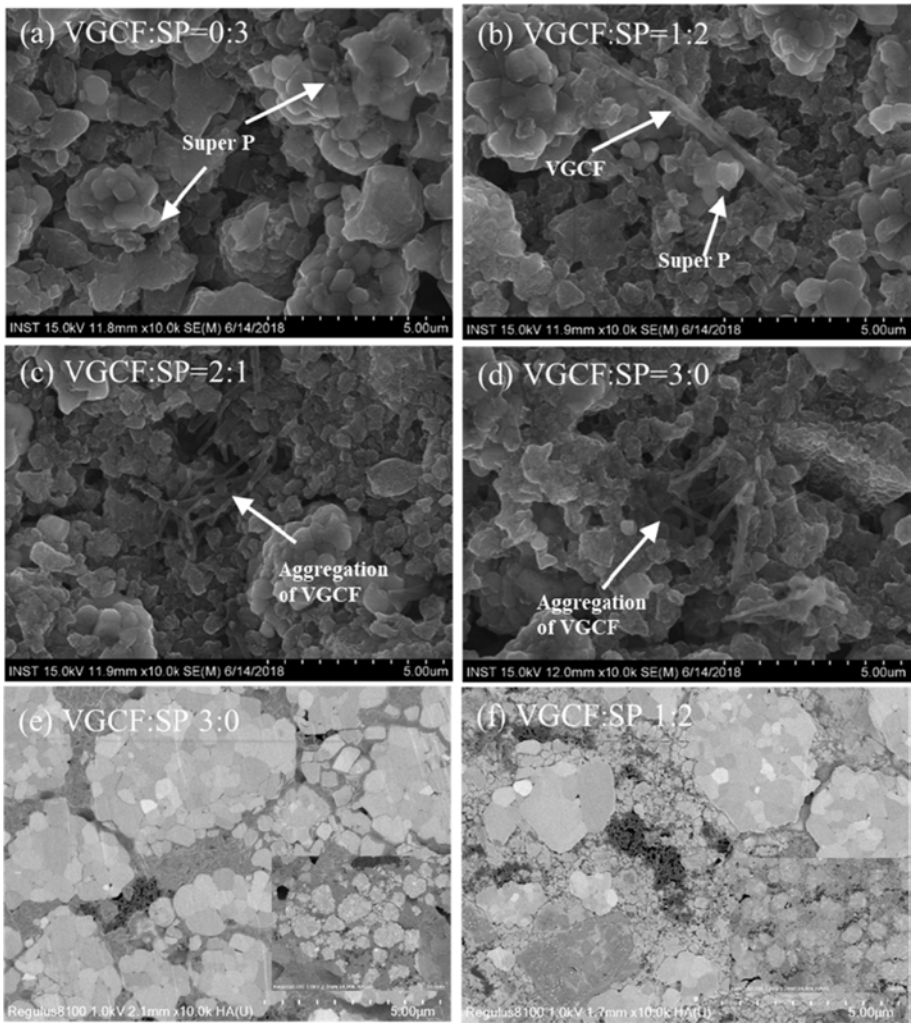

Fig. 7. SEM images of an 80% NCM cathode using diverse ratios of VGCF/SP as conductive additives (a-d) and cross-sectional SEM images of a sheet-type 80% NCM cathode using VGCF:SP 3:0 and 1:2 (e, f).

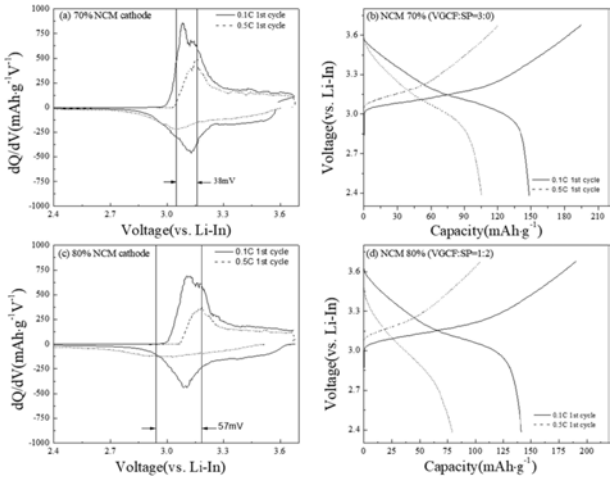

Fig. 8. dQ/dV curve for a 70% NCM cathode with VGCF/SP 3:0 and an 80% NCM cathode with VGCF/SP 1:2 (a, c) and initial charge-discharge curves at 0.1C and 0.5C (b, d).

lower electrode polarization, good rate capability, and better cycle retention than other samples.

To better understand formation of valid interfacial contact creating a functional conduction path between cathode elements, the microstructure of the 80% NCM cathodes was investigated, as in Fig. 7. Super P is observed on the NCM particle surface with agglomeration (Fig. 7(a)), whereas VGCF crosses between NCM particles creating an electron bridge (Fig. 7(b)). However, excess VGCF content results in self-agglomeration (Figs. 7(c) and (d)), which causes poor surface coverage and severe overpotential. Because of the reduced distance between adjacent NCM particles in the 80% NCM cathode, the contact area with VGCF is restricted by insufficient surface coverage characteristics despite agglomeration. On the other hand, using Super P as conductive additive can fill the spaces between NCM particles by self-aggregation.

Fig. 7(e) and 7(f) show the cross-sectional SEM image of VGCF/SP 3:0 and 1:2, respectively. Lack of contact point is an intrinsic drawback of VGCF due to its fibrous shape. For the same reason, it is not good at filling spaces between component particles. On the other hand, Super P added to the 80% NCM cathode can easily fill spaces by covering NCM particles. A consideration of

morphology and composition of conductive additives is important to enhance electrochemical performance of the cell.

The differential capacity curves (dQ/dV) of the 70% NCM cathode with VGCF and the 80% NCM cathode with VGCF/SP 1:2 as conductive additives derived from 0.1C and 0.5C charge-discharge curves in the voltage range of 2.38-3.68 V are shown in Fig. 8. Each composite cathode shows a sharp and high cathodic / anodic current peak that indicates lithium extraction and insertion, containing higher charge-discharge plateau. Although the broad peak and its corresponding lower plateau and small capacity are caused by overpotential at high current density, the lowest potential differences exhibited compare to others, indicating that the electrodes using VGCF/SP as conductive additives have the lowest electrode polarization and the best rate performance. This result suggests that the microstructure of a composite cathode can be controlled by proper selection of conductive additives to enhance electronic conductivity.

Conclusions

The effect of binary carbon additives (VGCF/SP) of different shape and size into sheet type NCM composite cathodes of all-solid-state batteries was investigated. The 70% NCM cathode with VGCF showed superior rate performance by connecting long range positioned NCM particles. As content of active material increased to 80% and the amount of inactive material (solid electrolytes and conductive additives) decreased, nano-sized Super P was a more appropriate selection to fill the closer intervals between NCM particles despite its agglomeration. Therefore, consideration of morphology and content of conductive additives according to the microstructure of the composite electrode is crucial in all-solid-state batteries to enhance rate capability and cycle life at high current density.

Acknowledgments

This work was supported by the Dual Use Technology Program of the Institute of Civil Military Technology Cooperation granted financial resources from the Ministry of Trade, Industry & Energy and Defense Acquisition Program Administration (17-CM-EN-11).

References

1. Y.S. Jung, D.Y. Oh, Y.J. Nam and K.H. Park, Isr. J. Chem. 55[5] (2015) 472-485.
2. C. Sun, J. Liu, Y. Gong, D.P. Wilkinson and J. Zhang, Nano Energy 33 (2017) 363-386.
3. A. Sakuda, A. Hayashi and M. Tatsumisago, Scientific reports 3 (2013) 2261.
4. S. Chen, D. Xie, G. Liu, J.P. Mwizerwa, Q. Zhang, Y. Zhao, X. Xu and X. Yao, Energy Storage Materials 14 (2018) 58-74.
5. Z. Gao, H. Sun, L. Fu, F. Ye, Y. Zhang, W. Luo and Y. Huang, Adv. Mater. 30[17] (2018) 1705702.
6. A. Sakuda, A. Hayashi and M. Tatsumisago, Current Opinion in Electrochemistry 6[1] (2017) 108-114.
7. J.K. Hong, J.H. Lee and S.M. Oh, J. Power Sources 111[1] (2002) 90-96.
8. I. Cho, J. Choi, K. Kim, M.-H. Ryou and Y.M. Lee, RSC Advances 5[115] (2015) 95073-95078.
9. J. Ma, B. Chen, L. Wang and G. Cui, J. Power Sources 392 (2018) 94-115.
10. R. Dominko, M. Gaberscek, J. Drofenik, M. Bele, S. Pejovnik and J. Jamnik, J. Power Sources 119 (2003) 770-773.
11. X. Bian, Q. Fu, C. Qiu, X. Bie, F. Du, Y. Wang, Y. Zhang, H. Qiu, G. Chen and Y. Wei, Mater. Chem. Phys. 156 (2015) 69-75.
12. S. Hong, J. Kim, M. Kim, X. Meng, G. Lee and D. Shin, Ceramics International 41[3] (2015) 5066-5071.
13. X. Li, X. Zhao, M.-S. Wang, K.-J. Zhang, Y. Huang, M.-Z. Qu, Z.-L. Yu, D.-s. Geng, W.-g. Zhao and J.-m. Zheng, RSC Advances 7[39] (2017) 24359-24367.
14. X. Bian, Q. Fu, C. Qiu, X. Bie, F. Du, Y. Wang, Y. Zhang, H. Qiu, G. Chen and Y. Wei, Materials Chemistry and Physics 156 (2015) 69-75.
15. K. Lee, S. Kim, J. Park, S.H. Park, A. Coskun, D.S. Jung, W. Cho and J.W. Choi, J. Electrochem. Soc. 164[9] (2017) A2075-A2081.
16. A. Sakuda, K. Kuratani, M. Yamamoto, M. Takahashi, T. Takeuchi and H. Kobayashi, J. Electrochem. Soc. 164[12] (2017) A2474-A2478.
17. J. Zhang, H. Zhong, C. Zheng, Y. Xia, C. Liang, H. Huang, Y. Gan, X. Tao and W. Zhang, J. Power Sources 391 (2018) 73-79.
18. Y.J. Nam, D.Y. Oh, S.H. Jung and Y.S. Jung, J. Power Sources 375 (2018) 93-101.
19. S. Boulineau, M. Courty, J.-M. Tarascon and V. Viallet, Solid State Ionics 221 (2012) 1-5.
20. A. Sakuda, H. Kitaura, A. Hayashi, K. Tadanaga and M. Tatsumisago, J. Electrochem. Soc. 156[1] (2009) A27-A32.
21. S. Choi, J. Kim, M. Eom, X. Meng and D. Shin, J. Power Sources 299 (2015) 70-75.
22. S. Noh, W.T. Nichols, C. Park and D. Shin, Ceramics International 43[17] (2017) 15952-15958.
23. S. Choi, S. Lee, J. Park, W.T. Nichols and D. Shin, Appl. Surf. Sci. 444 (2018) 10-14.